

tions compensates somewhat for the geometric effect. The disagreement between the expected and measured step height mentioned earlier may also be explained if each step is actually the sum of one (110) interplanar spacing and a CS plane. Although previous models of the reduced TiO₂(110) surface have not considered the possible existence of CS planes or their effect on the titania surface structure (8), the existence of these planar defects has been proposed by Firment and co-workers (9) to explain angle-resolved ultraviolet photoelectron spectroscopy (UPS) data from the reduced MoO₃(010) surface, another transition metal oxide surface that forms a variety of CS structures.

The spacing of the rows in Fig. 2 suggests that every sixth anion (121) plane is a CS plane and that the local composition in this area is Ti₃O₅, while the spacing of the rows in Fig. 3 suggests that CS occurs at every twelfth anion (1 $\bar{2}$ 1) plane and that the local composition is Ti₆O₁₁. Although these phases are known to have a higher conductivity than rutile, they are still semiconducting, a fact verified by tunneling spectroscopy measurements. The 0.2 Å corrugations within the rows of Fig. 2 have a 3.4 Å spacing, which is very close to the spacing of Ti atoms (3.5 Å) along this same direction in the ideal rutile unit cell. Apparently, the nearest neighbor Ti atoms, separated by only 3 Å along the *c* axis, are not resolved. The distance between adjacent units within the rows of Fig. 3, measured parallel to the [110] direction, is approximately 6.4 Å, close to the bulk rutile unit cell spacing in that direction (6.5 Å). The distance between adjacent units in the [113] direction is 5.6 Å, which is the distance between the neighboring Ti atoms in that direction. However, each Ti atom is clearly not imaged, and a more detailed model for the atomic structure within the rows will have to be formed on the basis of additional experiments.

REFERENCES AND NOTES

1. M. D. Kirk *et al.*, *Science* **242**, 1673 (1988); N. J. Zheng, U. Knipping, I. S. T. Tsong, W. T. Petuskey, J. C. Barry, *J. Vac. Sci. Technol. A* **6**, 457 (1988); E. Garfunkel *et al.*, *Science* **246**, 99 (1989); X. L. Wu, Z. Zhang, Y. L. Wang, C. M. Lieber, *ibid.* **248**, 1211 (1990).
2. M. L. Norton, J. G. Mantovani, R. J. Warmack, *J. Vac. Sci. Technol. A* **7**, 2898 (1989).
3. L. A. Bursill and B. G. Hyde, *Prog. Solid State Chem.* **7**, 177 (1972).
4. S. E. Gilbert and J. E. Kennedy, *J. Electrochem. Soc.* **135**, 2385 (1988); K. Itaya and E. Tomita, *Chem. Lett.*, 285 (1985); K. Sakamaki, S. Matsunaga, K. Itoh, A. Fujishima, Y. Gohshi, *Surf. Sci.* **219**, L531 (1989); S. E. Gilbert and J. H. Kennedy, *Langmuir* **5**, 1412 (1989); *Surf. Sci.* **225**, L1 (1990).
5. The 1.0 mm by 5 mm by 1.6 mm titania sample was oriented to within $\pm 0.5^\circ$ of the (110) face by Laue diffraction and cut with a high-speed diamond saw from a single-crystal boule. The surface was polished by sequential reduction of the size of Al₂O₃ grinding media down to 1 μ m. We reduced the crystal in UHV by annealing in a resistively heated Ta boat at a temperature above 900 K (on the basis of color) for 36 hours. After this treatment, the crystal was opaque and dark gray in color. The surface was then argon-ion-milled for 5 min at 2 kV and then subjected to 25 min of ion bombardment at 500 V using an estimated current density of 5 to 10 μ A/cm². The crystal was then annealed at 823 K for 30 min in 1×10^{-7} torr of oxygen in order to reoxidize the surface and anneal out the damage produced by ion bombardment.
6. No UPS data were taken on this surface, although the LEED patterns were similar to those on the TiO₂(110) surfaces that exhibit no band gap defect surface states; see H. R. Sadeghi and V. E. Henrich, *Appl. Surf. Sci.* **19**, 330 (1984).
7. For details on the determination of the apparent barrier height, see J. K. Gimzewski and R. Moller, *Phys. Rev. B* **36**, 1284 (1987); N. D. Lang, *ibid.*, p. 8173; G. Rohrer and D. Bonnell, *J. Am. Ceram. Soc.*, in press.
8. W. Göpel, G. Rocker, R. Feierabend, *Phys. Rev. B* **28**, 3427 (1983); V. Henrich, *Rep. Prog. Phys.* **48**, 1481 (1985).
9. L. E. Firment, A. Ferretti, M. R. Cohen, R. P. Merrill, *Langmuir* **1**, 166 (1985).
10. Supported at the University of Pennsylvania by IBM Research and the NSF and at Yale University by NSF solid state chemistry division grant DMR-8711423. We thank Z. Zhang for assistance in preparing the sample surface.

12 July 1990; accepted 26 September 1990

Surface Displacements in the 1906 San Francisco and 1989 Loma Prieta Earthquakes

PAUL SEGALL AND MIKE LISOWSKI

The horizontal displacements accompanying the 1906 San Francisco earthquake and the 1989 Loma Prieta earthquake are computed from geodetic survey measurements. The 1906 earthquake displacement field is entirely consistent with right-lateral strike slip on the San Andreas fault. In contrast, the 1989 Loma Prieta earthquake exhibited subequal components of strike slip and reverse faulting. This result, together with other seismic and geologic data, may indicate that the two earthquakes occurred on two different fault planes.

IN ORDER TO UNDERSTAND FULLY THE tectonic setting of the 17 October 1989 *M_s* 7.1 Loma Prieta earthquake and the implications of this event for earthquake hazard assessment it is important to understand its relation to the most recent large earthquake on this part of the San Andreas fault system, the great 1906 San Francisco earthquake. In this report, we recalculate the horizontal surface displacements accompanying the 1906 earthquake as determined by historical triangulation measurements. We contrast the 1906 deformation in the Loma Prieta region with that occurring in the October 1989 earthquake and discuss the implications of these results for earthquake recurrence estimates and for future earthquake hazards in the Santa Cruz Mountains.

Much of what is known about the 1906 earthquake has come from analysis of geodetic survey measurements (1). The surveys consisted of horizontal angle measurements, made with a theodolite, taped baselines, and astronomic azimuth sightings. Pre-earthquake surveys were conducted in the San Francisco Bay region in the 1850s and 1880s; the region was resurveyed following the earthquake in 1906 and 1907 (1906–7).

P. Segall, Geophysics Department, Stanford University, Stanford, CA 94305, and U.S. Geological Survey, Menlo Park, CA 94025.
M. Lisowski, U.S. Geological Survey, Menlo Park, CA 94025.

In 1908 Hayford and Baldwin (2) published displacement vectors found by taking the difference of coordinates derived from the 1906–7 survey and coordinates derived from earlier measurements. Their results showed that displacements of several meters parallel to the San Andreas fault extended many kilometers from the fault trace. At the northern (Point Reyes) and southern (Monterey Bay) ends of the network, however, many of the displacement vectors derived by Hayford and Baldwin are opposite to the right-lateral motion observed across the San Andreas fault.

We suggest that the anomalous displacements reflect computational limitations rather than measurement errors. In the 1908 calculations it was assumed that Mount Diablo, Mocho, and Santa Ana, located 20 to 40 km east of the San Andreas fault (Fig. 1), did not move during the earthquake. Errors accumulate with distance from these arbitrarily fixed stations, and any true motion of these sites would bias the calculated displacements. Computational limitations prevented simultaneous inversion of all the data and also prevented determination of confidence intervals.

Given the considerable advances in computing in the last 80 years, we can adopt a different strategy. We reanalyzed the data using only repeated horizontal-angle and astronomic azimuth measurements, forego-

ing the less accurate distance determinations. The relative displacements of three survey points (between the post-earthquake and pre-earthquake surveys) can be simply related to the change in the enclosed angle (3). We then used a generalized matrix inverse to solve for the displacements in terms of the measured angle and azimuth changes. The result is not unique because the data do not constrain some components (null vectors) of the displacement field. The null vectors are constrained by prior information, and this process yields a so-called "model coordinate solution" (4). Our prior model was a simple elastic dislocation model of the earthquake (5).

In order to eliminate effects of the 1868 earthquake (located on the Hayward fault) and the 1865 earthquake (thought to be located in the Santa Cruz Mountains) we first solved for the displacements of the ten stations (6) that were surveyed in the 1880s and again in 1906–7. These stations were connected by 20 angle changes and three astronomic azimuth changes. In this solution there are three null vectors corresponding to rigid body translation of the entire network in the two horizontal directions and uniform areal dilatation. Rigid body rotation of the network is controlled by the astronomic azimuths. We then computed the displacements of the remaining stations using angle changes from the 1850s to 1906–7. Because these angle changes do not form a well-connected network, we fixed the displacements of the ten 1880s stations to the values determined by the analysis of the 1880s to 1906–7 data (7). The displacements of the 1850s stations are consequently less well determined (Fig. 1).

In contrast to the results of Hayford and Baldwin (2), the recalculated displacements (Fig. 1) are entirely consistent with right-lateral strike slip in the 1906 earthquake. Relative displacements vary considerably along the strike of the fault decreasing from 5 to 6 m on the Point Reyes Peninsula to 3 to 4 m on the San Francisco Peninsula. The station at Loma Prieta, in the middle of what was to become the rupture zone of the 1989 earthquake, displaced slightly more than 1 m parallel to the trace of the San Andreas fault. This motion indicates that more than 2 m of strike slip occurred on this part of the fault in 1906 (8).

Horizontal displacements during the 1989 Loma Prieta earthquake have been measured with a variety of techniques. Most of the information has come from laser electronic distance measurements (EDM) (9). Changes in distance constrain horizontal displacements up to rigid body translations and rotations of the network (4). Global Positioning System (GPS) measure-

ments between Loma Prieta and stations Eagle, Allison, Mount Hamilton, and Fort Ord constrain the relative displacement vectors between these sites and thus the rotational component of the displacement field. The displacement of the Fort Ord site relative to stations remote from the epicentral region has been determined by Very Long Baseline Interferometry (VLBI) (10), constraining the translational components of the displacement field. A least-squares estimate of the horizontal displacements during the 1989 earthquake from the available EDM, GPS, and VLBI measurements is shown in Fig. 2 (11).

It is obvious that the displacement of

Loma Prieta was markedly different in magnitude and orientation during the 1989 and 1906 earthquakes (Fig. 2). In 1989 Loma Prieta moved 0.19 m, 0.15 m parallel to the fault and 0.11 m perpendicular to the fault. This oblique motion is reflected in results from uniform-slip elastic dislocation models, which yield a ratio of strike-slip to dip-slip motion of 1.4 (9). In contrast, during the 1906 earthquake, Loma Prieta was displaced 1 m parallel to the fault. The difference in the magnitude of the displacement is because there was more shallow slip in 1906 than in 1989. The difference in orientation means that sense of slip in the two earthquakes must have been distinctly different.

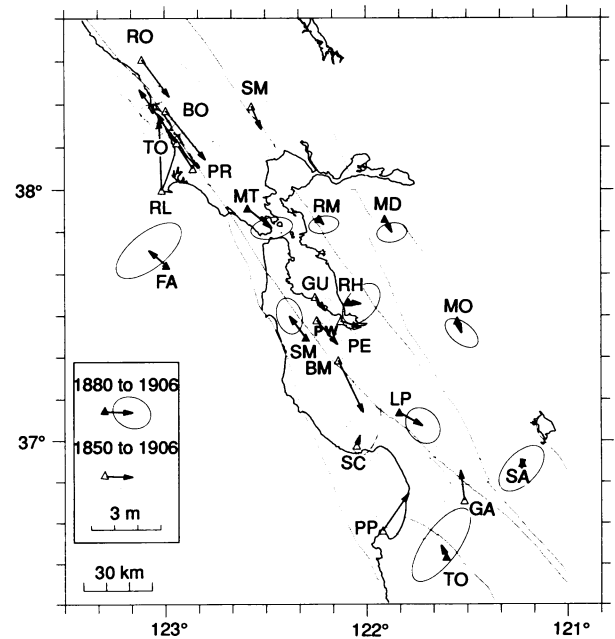


Fig. 1. 1906 San Francisco earthquake displacements. Displacements from the 1880s to 1906–7 and the 1850s to 1906–7 are distinguished by different symbols. Ellipses represent 95% confidence intervals. FA, Farallon lighthouse; MT, Mount Tamalpais; RM, Rocky Mound; MD, Mount Diablo; RH, Red Hill; SM, Sierra Morena; MO, Mocho; LP, Loma Prieta; SA, Santa Ana; TO, Mount Toro; PE, Pulgas East; PW, Pulgas West; GU, Guano; PR, Point Reyes. Other stations also referenced by two letter codes [see (2)].

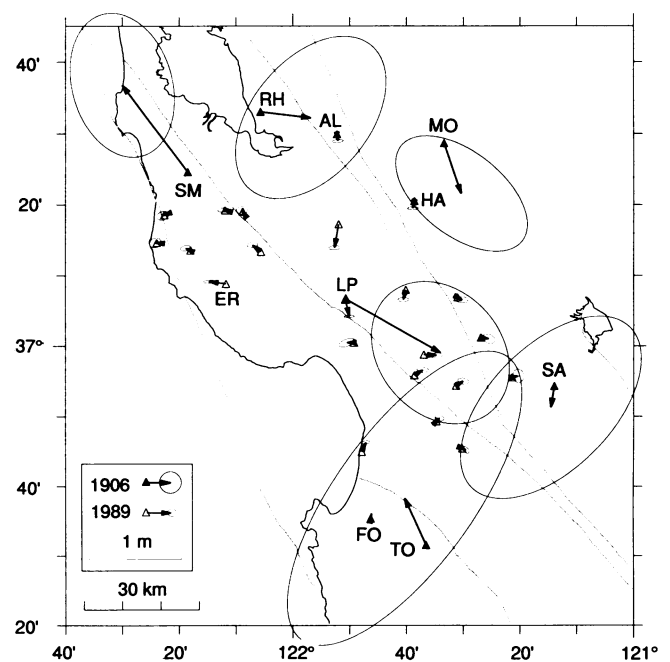


Fig. 2. 1989 Loma Prieta earthquake displacements (small error ellipses, 95% confidence intervals) compared to 1880s to 1906–7 displacements (large error ellipses). The 1989 displacements are from a joint solution with currently available EDM measurements, and GPS, and VLBI vectors. SM, Sierra Morena; RH, Red Hill; AL, Allison; MO, Mocho; HA, Mount Hamilton; LP, Loma Prieta; ER, Eagle Rock; SA, Santa Ana; FO, Fort Ord; TO, Mount Toro.

Elastic dislocation models indicate that the 1906 displacements can be adequately fit by pure strike-slip movement on either a vertical fault or a fault dipping 70° to the southwest, as in the 1989 Loma Prieta earthquake. Allowing both strike and dip slip adds a small component of normal slip, opposite to the observed reverse slip in the 1989 earthquake, but does not significantly improve the data fit. Furthermore, if the ratio of strike slip to reverse dip slip in the Loma Prieta segment is set equal to that observed in the 1989 earthquake, the fit to the 1906 data is significantly degraded (12). The observation that the displacement of Loma Prieta was so different in the two earthquakes means that the slip directions must have been different in the two events.

This interpretation is further supported by the difference in the long-term rates of horizontal and vertical displacement. At the latitude of Loma Prieta the San Andreas fault accommodates ~ 20 mm/yr of the horizontal motion between the North American and Pacific plates (13). The rate of vertical motion, as evidenced by the rate of uplift of marine terraces along the Santa Cruz coastline, is roughly 0.5 mm/yr (14). Even though the Loma Prieta segment of the fault is misoriented with respect to the relative plate motion vector, horizontal displacement rates exceed vertical rates by more than an order of magnitude. As noted by others, this means that earthquakes such as the 1989 Loma Prieta event with subequal amounts of strike slip and reverse slip must be relatively infrequent (15) and that predominantly strike-slip earthquakes, such as the 1906 event, must account for the bulk of the horizontal plate motion.

If the 1906 and 1989 earthquakes occurred on the same fault plane, then the difference in the orientation of the two slip vectors presents a problem. As long as the slip occurred in the direction of the resolved shear stress acting on the fault, the shear stress would have to have built up in a horizontal sense before 1906 and then rotated, so that between 1906 and 1989 stress accumulation on the fault was oriented at $\sim 35^\circ$ from the horizontal. Although such a rotation is not impossible, the observation that fault slip rates are nearly constant over thousands of years (16) implies that the loading process is nearly steady state.

Although models of the 1906 earthquake with pure strike slip in the upper 4 to 5 km and either no slip or oblique right reverse slip below this depth are consistent with the geodetic data, they are inconsistent with the geology if this slip pattern is repeated over any length of time. As discussed above, the long-term slip must be dominantly right-

lateral strike slip at all depths. Furthermore, a change in slip vector from strike slip to oblique slip at a depth of 5 km results in an incompatible strain field unless another fault takes up the reverse slip component at shallower depths.

The different mechanisms in 1906 and 1989 present no problem, however, if the two earthquakes occurred on two separate faults with different dips. Recently, Olson (17) found evidence in the microseismicity for a vertical fault distinct from the southwest-dipping Loma Prieta rupture plane. She relocated earthquakes in the Loma Prieta region for the 10 years before the 1989 earthquake. Surprisingly, the data show no evidence of a 70° southwest-dipping plane. Instead, the seismicity weakly outlines a vertical plane extending beneath the mapped trace of the San Andreas fault. This plane may represent the fault that ruptured in 1906.

A vertical strike-slip fault (the San Andreas) and a 70° dipping fault (the Loma Prieta rupture) with the same strike can both be driven by a temporally and spatially uniform stress. There are a family of applied stress states consistent with the observed rakes in the two earthquakes. Maximum compression directions can range from 64° from the fault if the intermediate (vertical) and minimum principal stresses are equal, to $<90^\circ$ if the intermediate and maximum principal stresses are equal (18).

The geodetic, geologic, and seismic data, suggest that the 1906 earthquake resulted from pure strike slip on a vertical San Andreas fault, whereas the 1989 Loma Prieta earthquake resulted from oblique slip on a separate, southwest dipping fault. If correct, this conjecture has extremely important implications for the evaluation of recurrence models and for present earthquake hazard. Before the Loma Prieta earthquake, several groups estimated earthquake recurrence times for this region using the "time predictable model" (19). In this model the earthquake repeat time is estimated by the slip in the most recent event divided by the long-term slip rate on the fault. There has been some controversy over whether it is more appropriate to use reported surface offsets of 0.4 to 1.5 m, or the geodetic slip estimates of ~ 2.5 m for slip in 1906. Using the smaller surface offsets yields a shorter repeat time, ~ 75 years, versus ~ 125 years using the geodetic estimates. As shown above, Loma Prieta was displaced 1 m parallel to the fault in 1906. Because of the proximity of this site to the fault, there must have been somewhat more than 2 m of slip at shallow to intermediate depths in 1906. Thus, our analysis supports the earlier interpretations of the geodetic data (5).

More importantly, if the Loma Prieta earthquake occurred on a separate fault, then it is not at all clear that simple recurrence models are appropriate. Although one could argue that strain energy is released in some volume of the earth's crust and therefore it does not matter which fault the slip takes place on, we consider that the earlier forecasts should be reevaluated if indeed the Loma Prieta earthquake did not occur on the predicted fault. Finally, if the vertical San Andreas fault did not slip in 1989, we should not dismiss the potential for a future earthquake on this structure (20). Although the 1989 earthquake must have decreased shear stress on a vertical San Andreas fault at some depths, it presumably concentrated stress at shallow to intermediate depths.

In summary, geodetic, seismic, and geologic data are consistent with the notion that the 1906 earthquake resulted from horizontal slip on a vertical fault, whereas the 1989 earthquake resulted from oblique slip on a separate southwest-dipping fault. If correct, this interpretation implies that earlier recurrence estimates should be reassessed and that the present earthquake hazard in the Santa Cruz Mountains is not negligible.

REFERENCES AND NOTES

1. H. F. Reid, in *The California Earthquake of April 18, 1906, Report of the State Earthquake Investigation Commission*, A. C. Lawson, Ed. (Carnegie Institution of Washington, Washington, DC, 1910), vol. II, pp. 3-55; W. Thatcher, *J. Geophys. Res.* **84**, 4862 (1975).
2. J. F. Hayford and A. L. Baldwin, in *The California Earthquake of April 18, 1906, Report of the State Earthquake Investigation Commission*, A. C. Lawson, Ed. (Carnegie Institute of Washington, Washington, DC, 1908), vol. I, pp. 114-145.
3. The change in horizontal angle ($\angle AOB$) $\delta\theta$ is

$$\delta\theta = \frac{\sin(\alpha_1)}{R_1} (u_1^O - u_1^A) + \frac{\cos(\alpha_1)}{R_1} (u_2^O - u_2^A) - \frac{\sin(\alpha_2)}{R_2} (u_1^O - u_1^B) + \frac{\cos(\alpha_2)}{R_2} (u_2^O - u_2^B)$$
 where u_j^i is the displacement of station i in the j direction, and α_j and R_j are the angle (from x_1) and length of the vector from the vertex station (O) to station A and B, respectively, and $\theta = \alpha_1 - \alpha_2$.
4. P. Segall and M. V. Matthews, *J. Geophys. Res.* **93**, 14,954 (1988).
5. The a priori model is essentially equivalent to that given by W. Thatcher and M. Lisowski, *ibid.* **92**, 4771 (1987).
6. Farallon lighthouse, Mount Tamalpais, Rocky Mound, Mount Diablo, Red Hill, Sierra Morena, Mocho, Loma Prieta, Santa Ana, and Mount Toro.
7. There are 38 angle changes between the 1850s and 1906-7 employed to determine the displacements of 13 additional stations. There is one additional null vector in this solution corresponding to dilatation of the lines between Red Hill and stations Pulgas East Base, Pulgas West Base, and Guano. In all of these calculations the angle changes are assumed to be independent.
8. For a simple screw dislocation in an elastic half-space with slip s from the earth's surface to depth d , the displacement decays with distance from the fault x according to $u = (s/\pi)\tan^{-1}(d/x)$. For slip to a depth

- of 10 km, this gives a slip of 2.9 m for 1.2 m of slip at Loma Prieta ($x \approx 3$ km). A more precise three-dimensional dislocation calculation yields a slip of 2.5 ± 0.4 m from the surface to 10 km.
9. M. Lisowski, W. H. Prescott, J. C. Savage, M. J. Johnston, *Geophys. Res. Lett.* **17**, 1437 (1990).
 10. T. A. Clark *et al.*, *ibid.*, p. 1215.
 11. The EDM measurements were made to station Eagle; the GPS occupations were at Eagle Un, ~40 m away. In the calculation the two markers were treated as one. On Loma Prieta the GPS occupations and the south-directed EDM lines were from LP1, whereas the EDM lines to the north were from Loma USE. We have corrected all measurements to LP1. For this solution there are 59 observations, 46 unknowns (2 for each of 23 stations), and no null space.
 12. For strike slip on a vertical dislocation extending from the earth's surface to depths of 5 to 15 km, the mean-square lack of fit [the residual sum of squares corrected for misclosure; see (4)] is 1.4. For strike slip on a plane dipping 70° to the southwest the mean-square lack of fit is 1.5. Both models provide acceptable fits to the data. W. Thatcher and G. Marshall [*Eos* **17**, 554 (1990)] presented similar results. In contrast, if the slip vector is constrained so that the strike-slip component is 1.4 times the dip-slip component, the mean-square lack of fit is 2.8, a significantly poorer fit. With 18 linearly independent observations and three parameters, models with mean-square lack of fit greater than 1.7 are rejectable at the 95% confidence level. The variance in the triangulation measurements estimated from the network misclosure is completely consistent with the a priori estimate of the data variance.
 13. Near Loma Prieta a total of 33 to 38 mm/yr of slip is partitioned between the San Andreas and Calaveras faults. Estimates of slip on the San Andreas fault range from 13 mm/yr [W. H. Prescott, M. Lisowski, J. C. Savage, *J. Geophys. Res.* **86**, 10,853 (1981)] to 26 mm/yr [M. Mats'ura, D. D. Jackson, A. Cheng, *ibid.* **91**, 12,661 (1986)].
 14. W. C. Bradley and G. B. Griggs [*Geol. Soc. Am. Bull.* **87**, 433 (1976)] estimated uplift rates of as much as 0.26 mm/yr. T. C. Hanks, R. C. Bucknam, K. R. Lajoie, and R. E. Wallace [*J. Geophys. Res.* **89**, 5771 (1984)] estimated an uplift rate of 0.35 mm/yr. All rates apply to the Santa Cruz coastline, the uplift rate at the fault trace is not well known.
 15. R. S. Anderson, *Science* **249**, 397 (1990); Valensise and Ward, in preparation.
 16. The average rate of slip on the San Andreas fault in the Carrizo Plains has been 33.9 ± 2.9 mm/yr during the last 3,700 years and $35.8 + 5.4/-4.1$ mm/yr during the last 13,250 yr [K. E. Sieh and R. H. Jahns, *Geol. Soc. Am. Bull.* **95**, 883 (1984)]; the geodetically determined slip-rate somewhat north-west on the creeping segment of the fault has been 33 ± 1 mm/yr over the last 100 years [W. Thatcher, *J. Geophys. Res.* **84**, 2283 (1979)].
 17. J. Olson, *Geophys. Res. Lett.* **17**, 1492 (1990).
 18. As pointed out by T. Heaton (personal communication). Erect a coordinate system with x'_1 horizontal and normal to fault strike, x'_2 horizontal and parallel to fault strike, and x'_3 vertical. The condition that the vertical fault be pure strike-slip is $\sigma'_{13} = 0$. If we assume that one principal stress is near vertical, then σ'_{23} must also vanish. The horizontal and vertical shear stresses acting on the dipping fault are given by $\tau_h = \sigma'_{12} \sin(\delta)$ and $\tau_v = (\sigma'_{11} - \sigma'_{33}) \sin(\delta) \cos(\delta)$, where δ is the fault dip. Consider the intermediate principal stress (σ_2) to be vertical and the minimum compression (σ_3) to be at an angle θ clockwise from x'_1 . The observed rake of the slip vector in the Loma Prieta earthquake requires that $\tau_h = \beta \tau_v$; $\beta \sim 1.4$ or $\phi = \sin^2(\theta) - \sin(\theta) \cos(\theta) / \beta \cos(\delta)$ where the parameter $\phi = (\sigma_2 - \sigma_3) / (\sigma_1 - \sigma_3)$ describes the shape of the stress ellipsoid. Note that $\phi \geq 0$, as required by definition, for $\theta \geq \tan^{-1}[1/\beta \cos(\delta)] \approx 64^\circ$. The direction of maximum compression, consistent with the slip vector in the two earthquakes, ranges from $64^\circ \leq \theta < 90^\circ$. The minimum value of θ (N16°E) occurs when $\sigma_2 = \sigma_3$, the maximum (N42°E) when $\sigma_2 = \sigma_1$.
 19. A. G. Lindh, *U.S. Geol. Surv. Open-File Rep.* **83-63** (1983); L. R. Sykes and S. P. Nishenko, *J. Geophys.*

Res. **89**, 5905 (1984); C. H. Scholz, *Geophys. Res. Lett.* **12**, 17 (1985).

20. H. Kanamori (personal communication) pointed out that the two 1985 Nahani earthquakes, M_s 6.6 (October 1985) and M_s 6.9 (December 1985) had epicenters only 2 to 3 km apart, coincident after-shock zones, and similar focal mechanisms; these common features suggest that they either ruptured the same plane or closely spaced parallel planes; R. J. Wetmiller *et al.*, *Bull. Seismol. Soc. Am.* **78**, 590 (1988); G. L. Choy and J. Boatwright, *ibid.*, p.

1627.

21. We thank R. Kovach, T. Heaton, and H. Kanamori for valuable discussions; D. Richards, C. Williams, and Y. Du for assistance in the numerical calculations; J. Savage, W. Thatcher, D. Oppenheimer, G. Beroza, B. Ellsworth, and K. Lajoie for comments. This work was supported by the U.S. Geological Survey and by National Science Foundation grant EAR 90-03575 to Stanford University.

23 July 1990; accepted 19 October 1990

Modern Cyanobacterial Analogs of Paleozoic Stromatoporoids

JÓZEF KAŹMIERCZAK AND STEPHAN KEMPE

Recent and subfossil calcareous structures resembling cystose and subclathrate Paleozoic stromatoporoids have been discovered in a sea-linked, stratified, alkaline crater lake on Satonda Island, Indonesia. The structures are produced by mats of coccoid cyanobacteria growing along the lakeshore from the water surface down to the O_2 - H_2S interface located at a depth of 22.8 meters. Calcification of the mats is controlled by seasonal changes in calcium carbonate supersaturation in the epilimnion. The internally complex structures are a product of two different calcification processes: (i) periodic in vivo calcification of the surficial cyanobacterial layers by low-Mg calcite, and (ii) early postmortem calcification of the cyanobacterial aggregates below the mat surface by microbially precipitated aragonite. The finding supports the idea that Paleozoic stromatoporoids represent fossilized cyanobacteria (stromatolites). It also implies that the stromatoporoid-generating epicontinental seas during the early Paleozoic may have been more alkaline and had a higher carbonate mineral supersaturation than modern seawater.

STROMATOPOROIDS ARE CALCAREOUS marine fossils common in many lower Paleozoic shallow-water carbonate deposits. The characteristic specimens came from Devonian limestones in Germany (1). These true stromatoporoids occur in mid-Ordovician to lowermost Carboniferous (Strunian) rocks. Most of the upper Paleozoic and Mesozoic fossils ascribed to stromatoporoids are sponges, predominantly calcified demosponges known as sclerosponges or coralline sponges (2, 3). They differ significantly from the Paleozoic stromatoporoids in their skeletal architecture, microstructure, and in the presence of spicules. Such pseudo-stromatoporoid fossils have been usually treated as separate groups and have been variously named Disjectoporida, Sphaeractinoidea, and Spongiomorpha (4). The practice of calling them stromatoporoids (3, 5, 6) should be abandoned because it is misleading.

Paleozoic stromatoporoids have been ascribed to various groups of organisms, in recent years to coelenterates (mostly hydro-

zoans) (7) and sponges (particularly sclerosponges) (8). No conclusive evidence for such affinities has been presented, however. Stromatoporoids have also been hypothesized (9) to form from in vivo calcification of coccoid cyanobacterial mats comparable to certain fossil and recent calcareous stromatolites. This suggestion has been supported by findings of remnants of coccoid cyanobacteria within skeletal elements of various stromatoporoids (10). Because living stromatoporoid-like stromatolites have not been found, the main question of this hypothesis is how the calcifying mats could produce the diversified and in many cases quite regular patterns that characterize many stromatoporoids. Some workers have suggested that these patterns are too advanced to be products of prokaryotic organisms (11).

In this report we describe modern calcified cyanobacterial mats that closely resemble certain Paleozoic stromatoporoids. These mats were discovered in the crater lake on Satonda Island (Indonesia) during the Indonesian-Dutch SNELLIUS II Expedition in November 1984, and we studied them in detail during the Indonesian-German SONNE 45B cruise in the fall of 1986 (12).

Satonda Island, ~2 km in diameter, is

J. Kaźmierczak, Institute of Paleobiology, Polish Academy of Sciences, Al. Zwirki i Wigury 93, PL-02089 Warszawa, Poland.

S. Kempe, Institute of Biogeochemistry and Marine Chemistry, University of Hamburg, Bundesstrasse 55, D-2000 Hamburg 13, Germany.